

# Radio Lobes of Pictor A: an X-ray spatially resolved Study

Giulia Migliori

*Dipartimento di Astronomia, Università di Bologna, via Ranzani 1, 40127 Bologna, Italy*  
*Istituto di Astrofisica e Fisica Cosmica-Bologna, INAF, Via Gobetti 101, I-40129*  
*Bologna, Italy*  
*SISSA/ISAS, Via Beirut 2-4, I-34014, Trieste, Italy*

migliori@iasfbo.inaf.it

Paola Grandi

*Istituto di Astrofisica e Fisica Cosmica-Bologna, INAF, Via Gobetti 101, I-40129*  
*Bologna, Italy*

grandi@iasfbo.inaf.it

Giorgio G.C. Palumbo

*Dipartimento di Astronomia, Università di Bologna, via Ranzani 1, 40127 Bologna, Italy*  
 giorgio.palumbo@unibo.it

Gianfranco Brunetti

*Istituto di Radioastronomia-Bologna, INAF, Via Gobetti 101, I-40129 Bologna, Italy,*  
 g.brunetti@ira.inaf.it

Carlo Stanghellini

*Istituto di Radioastronomia-Bologna, INAF, Via Gobetti 101, I-40129 Bologna, Italy,*  
 c.stanghellini@ira.inaf.it

## ABSTRACT

A new *XMM-Newton* observation has made possible a detailed study of both lobes of the radio galaxy Pictor A. Their X-ray emission is of non thermal origin and due to Inverse Compton scattering of the microwave background photons by relativistic electrons in the lobes, as previously found. In both lobes, the equipartition magnetic field ( $B_{eq}$ ) is bigger than the Inverse Compton value

( $B_{IC}$ ), calculated from the radio and X-ray flux ratio. The  $B_{eq}/B_{IC}$  ratio never gets below 2, in spite of the large number of reasonable assumptions tested to calculate  $B_{eq}$ , suggesting a lobe energetic dominated by particles.

The X-ray data quality is good enough to allow a spatially resolved analysis. Our study shows that  $B_{IC}$  varies through the lobes. It appears to increase behind the hot spots. On the contrary, a rather uniform distribution of the particles is observed. As a consequence, the radio flux density variation along the lobes appears to be mainly driven by magnetic field changes.

*Subject headings:* galaxies:individual (Pictor A) - radiation mechanisms: non-thermal - X-rays: galaxies

## 1. Introduction

With the advent of the space observatories, *Chandra* and *XMM-Newton*, fundamental progress in the study of X-ray emission from active galactic nuclei (AGNs) has become possible. X-ray spatially resolved studies of radio loud AGNs have been performed and those radiative processes, which are responsible for X-ray emission far from the nucleus, in the jets, hot spots and lobes, have been investigated.

In the last years many studies have been produced on each of these structures (Harris & Krawczynski 2000, Hardcastle et al. 2002, Croston et al. 2005, Kataoka & Stawarz 2005). The aim is to reach a clearer knowledge of the physics powering each component and of their relative interplay. Among the extended structures which emit X-ray photons, the lobes are the faintest and most difficult regions to detect. On the other hand, X-ray observations provide important physical information. In fact, it is thought that X-ray emission in the lobes is due to Inverse Compton (IC) by relativistic electrons. IC scattering in radio lobes can occur either between  $\gamma \approx 10^3$  electrons and CMB photons (Harris & Grindlay 1979, Miley 1980) or between  $\gamma \approx 100 - 300$  electrons and nuclear photons (Brunetti et al. 1997, 2000). The last case is more relevant in the context of powerful and compact ( $< 100$  kpc) radio galaxies. A comparison of the radio and X-ray fluxes provides a direct estimate of the average magnetic field ( $B_{IC}$ ) along the line of sight and, independently the number densities of the IC emitting particles in the lobes.

Two are the main concerns in this kind of study: good statistics (radio lobes are weak X-ray sources) and spatial resolution to distinguish non thermal from thermal emission. In fact it is possible that external gas, compressed by the expansion of the radio lobes, emits in the X-ray band by thermal bremsstrahlung (Kraft et al. 2000, Reynolds et al. 2001). Obviously the task is even more difficult if the radio galaxy is situated in a cluster. In

spite of these problems, X-ray detections of extended synchrotron radio regions were already been achieved focusing on low redshift radio galaxies (Feigelson et al. 1995, Kaneda et al. 1995, Brunetti et al. 1999, Tashiro et al. 2001). These early results from X-ray studies on lobes have opened a new field of research and in particular have allowed the first checks on the assumption of minimum energy condition in the lobe (equipartition). Several detections of Radio Lobes have been successively performed with Chandra and XMM-newton (Isobe et al. 2002, Grandi et al. 2003, Comastri et al. 2003, Hardcastle et al. 2005, Croston et al. 2005, Kakatoa & Stawarz 2005) and the equipartition condition has been further investigated. There is not yet a general agreement: in some cases a substantial concordance between equipartition and Inverse Compton magnetic field has been claimed (Brunetti et al. 2001, Hardcastle et al. 2002, Belsole et al. 2004, Croston et al. 2005, Overzier et al. 2005), in other cases a moderate violation of equipartition ( $B_{eq} > B_{IC}$ ) has been found (Brunetti et al. 1999, Isobe et al. 2002, Comastri et al. 2003, Grandi et al. 2003, Kataoka et al. 2003, Bondi et al. 2004). It is clear that slightly different assumptions drive to the two opposite results. The most reasonable conclusion is that the unbalance between the particle and magnetic field energy density is not dramatic and the equipartition argument is a viable zero-order reference guide.

The spatial distribution of both magnetic field and particles within the lobes themselves is a second connected branch of investigation. Specifically studying the variations of magnetic fields and particle densities with position turns out to be a useful procedure to get information on the dynamical plasma evolution. Observationally attempts in addressing these problems have been performed for only a few Radio Galaxies. The results indicate an enhancement of the magnetic energy density towards the edge of the lobes (Tashiro et al. 01, Isobe 2002, 2005 )

Pictor A , a famous nearby ( $z=0.035$ ) radio bright ( $P_{408MHz} = 6.7 \times 10^{26}$  W Hz $^{-1}$ ) Fanaroff Riley II (FRII) radio galaxy, is an excellent candidate for studying X-ray IC emission from the lobes. Actually, *XMM-Newton* discovered X-ray radiation associated to the extended radio lobes (Grandi et al. 2003). In spite of the relatively short exposure time ( $\sim 15$  ks) and the very high background, a reasonably good spectrum was obtained from a circular region centered on the east lobe. However, the data interpretation was not univocal, as the X-ray spectrum could be described by both a power law ( $\alpha_X = 0.6 \pm 0.2$ ) and a thermal model ( $kT \sim 5$  keV). The presence of an extended emission, most likely to be ascribed to non-thermal processes, has been recently confirmed (Hardcastle & Croston 2005).

In order to definitively solve the ambiguity about the nature of the radio-lobe X-ray emission, *XMM-Newton* re-pointed Pictor A on January 14, 2005. The observation was successful and, beyond our expectation, the MOS1 signal-to-noise ratio was good enough to

allow a spatially resolved spectral analysis of both the west and east radio lobes.

## 2. Data Reduction

The radio lobes were the target of the new *XMM-Newton* observation. For this reason, the EPIC/p-n and EPIC/MOS1 cameras operated in full-frame mode, with thin optical filter. The EPIC/MOS2 camera operated in small-window mode in order to assure the study of the nucleus without any pile up problem. P-n data were excluded because of a substantial problem with nuclear PSF, which covers a great fraction of the X-ray emission from the lobes. Therefore our study is only based on the MOS1 instrument data.

Data reduction was performed using the software package SAS, Version 6.0. A calibration index file appropriate for the date of the observation and data analysis (July 2005) was produced. We identified two high background periods (background flares) and we excluded all periods with a count rate higher than  $0.35 \text{ cts s}^{-1}$ . After the cleaning procedure, the net total exposure time was  $\sim 50 \text{ ks}$ . We selected only those events with **PATTERN**  $\leq 12$  (single, double, triple and quadruple events) and imposed the filter **#XMMEA\_EM** in order to exclude artifact events.

### 2.1. Selection of the studied regions

VLA observations (Perley et al. 1997) of Pictor A show two nearly circular radio lobes with hot spots and a faint radio jet connecting the nucleus to the west hot spot. The same features can be observed in Figure 1 (*Upper Panel*), where the MOS1 image (0.2-10 keV) is shown. If the 20 cm radio contours are superposed on the *XMM-Newton* image, the spatial coincidence between radio and X-ray emission is unambiguous. In particular, the X-ray counterparts of the radio lobes are clearly visible as elongated emission around the bright nucleus. In comparison with the previous *XMM-Newton* observation, performed in 2001 (Grandi et al. 2003), the good quality of this new data has allowed two different kinds of analysis. In fact, we studied each lobe as a whole, but also performed a *spatially resolved individual study* on both lobes. In the following, we give a description of the regions chosen for the two studies.

**The extended regions: E and W** – The selection of the studied regions was based on both X-ray and radio images. We selected two circular regions, one for each lobe, with different radius (r) (r=88" for the east lobe and r=100" for the west lobe). Afterwards we will refer to these two regions as **E** and **W** for east and west lobes, respectively. In order

to avoid any nuclear contamination we excluded the emission coming from a circular region of  $r=120''$  centered on the nucleus. This choice is also supported by considerations based on the calibration report by Ghizzardi (XMM-SOC-CAL-TN-0022). She clearly shows that 80% of the nuclear source emission is contained within about 30 arcsec. Moreover, following Ghizzardi's prescriptions we have evaluated encircled energy fraction for the nucleus in the case of an annulus comprising our selected lobe regions ( $R_{min}=120''$ ,  $R_{max}=222''$ ). The result is that any possible nuclear contamination should be of the order of the measured errors for the fluxes.

In the case of the west lobe, it was also necessary to exclude the jet emission (a circle with  $r=22''$ ) and a point-like source ( $r=15''$ ). The excluded regions are represented in Figure 1 (*upper panel*).

**The subregions** – In order to perform a spatially resolved study of the lobes, we selected rectangular subregions in each lobe, as shown in Figure 1 (*lower pane*). In what follows, we indicate these regions as **e1** , **e2** , **e3** for the east lobe, and **w1** , **w2** , **w3** for the west lobe, counting from top to bottom.

## 2.2. X-ray Spectral Analysis

We accumulated spectra of the two regions **E** and **W** , and of the subregions previously described, i.e. **e1** , **e2** , **e3** and **w1** , **w2** , **w3** in the energy range 0.2-10 keV. In each case, the background was extracted from a region of the same extension taken on the same CCD. Spectral analysis was conducted on two different levels. First, we maximized the statistics and considered the **E** and **W** spectra in order to define which radiative process is causing the X-ray emission. Afterwards, we analyzed the sub-region spectra. Spectral analysis has been done with XSPEC, Version 11.2.0. Every spectrum was grouped in order to ensure a minimum of 25 net counts in each bin. Throughout the paper, all errors are quoted at 90% confidence for two interesting parameters ( $\Delta\chi^2 = 4.61$ ).

## 2.3. Radio Fluxes

The radio fluxes of all the analyzed regions were derived at 20 cm from the VLA image produced by Perley et al. (1997). Uncertainties in measurements of flux density of extended structures are difficult to determine for interferometric data. Extended emission may be lost because the corresponding spacial frequencies are not sampled by the array of antennas. Furthermore this radio source is at low declination and the VLA observed it at a very low

elevation, with not negligible atmospheric opacity at this frequency. These effects have been taken in consideration by Perley et al. who find the VLA total flux density, after the standard calibration, of about 6% lower respect to the total flux density derived by single dish measurements. They ascribe this difference to the atmospheric opacity only, and correct the image accordingly. Given the considerations above the uncertainty in the flux density measurements is dominated by residual calibration errors which can be estimate to be about 3%.

### 3. E and W regions

#### 3.1. Thermal versus non-thermal emission

The first step of the study was aimed at solving the ambiguity (thermal vs non-thermal) about the origin of the lobes X-ray emission. Consequently, we tested two different models: a thermal emission from hot diffuse gas (*mekal* model in XSPEC, Mewe et al. 1985) and a non-thermal radiation modeled with a pure power law. In both cases, the acceptable range of  $N_H$  is consistent with the Galactic line-of-sight value  $N_H^{Gal} = 4.18 \times 10^{20} \text{ cm}^{-2}$ . Thus we fixed the column density to the Galactic value in order to reduce the parameters uncertainties. Results in Table 1 strongly suggest a non-thermal origin of the radiation. In each lobe a power law is preferred to a thermal model and the X-ray photon indeces are in very good agreement with the average radio slopes ( $\alpha_R \sim 0.8$ ) measured by Perley et al. (1997). The non-thermal X-ray flux of the east lobe is consistent with the previously reported one by Grandi et al. (2003), once it is rescaled to their (smaller) extraction area. However, to completely explore all the possibilities, a mixed of thermal (*mekal*) and non-thermal (power law) radiation was also tested to verify the presence of gas within the lobes. The dual component model does not significantly improve the fit. Even if present, the thermal component is negligible and its contribution to the the total 0.5 – 2 keV flux is not larger than 15%.

#### 3.2. Lobes Energetic

Having established the non-thermal nature of the X-ray emission, we could directly determine the magnetic field ( $B_{IC}$ ) in both lobes by assuming that the emission is due to IC scattering of CMB photons. If, the synchrotron radio ( $L_{syn}$ ) and Compton scattered X-ray ( $L_{IC}$ ) luminosities are known (e.g., Blumenthal & Gould 1970)

$$L_{syn} = C_{syn} k_e V B^{\alpha+1} \nu^{-\alpha} \quad (1)$$

and

$$L_{IC} = C_{IC} k_e V \nu^{-\alpha} \quad (2)$$

$B_{IC}$  can be immediately estimated

$$B_{IC} = \left[ \frac{F_{1.4 \text{ GHz}}}{F_{1 \text{ keV}}} \frac{C_{IC}(\alpha)(1+z)^{\alpha+3}}{C_{sin}(\alpha)} \right]^{\frac{1}{\alpha+1}} \left[ \frac{\nu_{syn}}{\nu_{IC}} \right]^{\frac{\alpha}{\alpha+1}}. \quad (3)$$

$C_{IC}$  and  $C_{syn}$  are quantities depending only from  $\alpha$  and  $V = A \times s$  is the volume,  $A$  being the area ( $\text{arcsec}^2$ ) projected on the sky plane and  $s$  the thickness of the analyzed region.  $k_e$  is the electron density having assumed a power law distribution for the electrons  $N(\gamma) = k_e \gamma^{-(2\alpha+1)}$  and  $\alpha = \Gamma - 1 = \alpha_x = \alpha_R$ .

$k_e$  can be derived from the synchrotron luminosity (1), and thus the lobe energetics, i.e. magnetic field and particles energy densities (respectively  $u_m$  and  $u_{e+p}$ ) can be estimated

$$u_m = \frac{B_{IC}^2}{8\pi} \quad (4)$$

$$u_{e+p} = \frac{(1+k)mc^2}{2\alpha-1} k_e (\gamma_{min})^{1-2\alpha}. \quad (5)$$

The ratio between electron and proton densities  $k$  was set equal to 1 and the low energy cut-off of the electron spectrum  $\gamma_{min} = 50$ . We also assumed  $\alpha = 0.8$ , as indicated by both radio and X-ray observations.

The results (Table 2) show very similar physical conditions in the two lobes (**E** and **W** regions). The strength of the magnetic field ( $B_{IC} \sim 3\mu G$ ) is the same in both lobes and no significant difference is found for the particle density  $k_e$ . Most relevant is the dominance of the particle energy density on the magnetic field energy density. Energetic of both lobes appears to be dominated by particles ( $u_{e+p}/u_m = (56 \pm 10)(\gamma_{min}/50)^{-0.6}$  for **E** and  $u_{e+p}/u_m = (50 \pm 10)(\gamma_{min}/50)^{-0.6}$  for **W**), confirming a possible departure from the equipartition principle.

We are aware that this is a very delicate point, since a large number of assumptions are necessary to estimate the lobe energetics. In Appendix we discuss the dependence on parameters,  $k$ ,  $\gamma_{min}$  and  $s$ , and show that the ratio between the equipartition and IC magnetic fields,  $B_{eq}/B_{IC}$ , when we consider plausible variations of these parameters, never goes below a factor of 2. Even considering a more complex particle distribution (a broken power law) the  $B_{IC}$  and  $B_{eq}$  discrepancy can not be reduced to a value less than  $\sim 1.6$  (Hardcastle & Croston 2005).

#### 4. Spatially resolved Analysis

The analysis performed on the whole lobes was successively extended to the sub-regions data set. Data of each subregion were fitted with a power law absorbed by Galactic  $N_H$ . Since the low number of counts (ranging from a minimum of 125 to a maximum of 216), the X-ray spectral slopes were poorly constrained and therefore we decided to fix  $\Gamma = 1.8$  in each sub-region. This choice allowed to better constrain the X-ray fluxes and to map physical quantities (namely magnetic field and particles) through the lobes, following the same procedure adopted in the previous section. The results are in Table 2. In spite of the quite large uncertainties, Table 2 suggests that  $B_{IC}$  increases behind the east hot spot, where the radio flux is higher (see *Lower Panel* of Fig. 2).

On the contrary, no change of the electron density appears evident.

Combining data from both lobes, the previous results are strengthened. In Figure 2,  $B_{IC}$  and  $k_e$  are plotted as a function of radio flux (divided for the corresponding sub-region volume).  $B_{IC}$  variation is statistically significant ( $\chi^2 = 4.7$  with a probability  $p = 3.0 \times 10^{-4}$ ) and traces the variation of the radio flux density. A *Spearman test* gives a correlation coefficient  $r = 0.8$  with a  $s = 0.0499$  significance.

Again no trend is found between  $k_e$  and the radio flux in Figure 2 (upper panel). The correlation test gives  $r = 0.31$  with  $s = 0.54$ .

We note that these conclusions are based on the hypothesis that the spectral energy distribution of the particles does not vary through the lobe, i.e. that our assumption of  $\Gamma - 1 = \alpha$  is valid for each sub-region analyzed. This is a very crucial point, as in principle spectral index variations among the analyzed sub-regions can affect the  $B_{IC}$  – radio flux trend (observed in Figure 2). In order to exclude this possibility, we analyzed the spectral index radio maps between 20 and 6 cm and between 6 and 2 cm (kindly provided by R. Perley and shown in Fig. 5 of Perley et al. 1997). The maps shows negligible spectral index variations ( $\Delta\alpha \leq 0.05$ ) from a sub-region to another one, confirming the robustness of our result.

The different behaviour of  $B_{IC}$  and  $k_e$  might indicate a dynamical decoupling between the magnetic field and the electron energy densities (i.e changes of the  $u_{e+p} / u_m$  ratio along the lobes) as found in 3C452 by Isobe et al. (2002, 2005). It is possible that the plasma expands along the regions immediately beyond the hot spots, while (high energy) electrons diffuse away on larger scales providing a fairly constant density distribution. An efficient spatial diffusion of the high energy electrons in the lobes and a decreasing magnetic field with distance from hot spots (yielding particles decoupling) was suggested by Blundell & Rawlings (2000) to explain the discrepancy between the radiative lifetimes of electrons and dynamical ages of double radio galaxies. In this case if relativistic energetic particles stream through the plasma replenishing the lobes, the synchrotron spectral steepening are driven



by the magnetic field decay during the plasma expansion rather than the emitting particles aging. Our results in Fig.2 are in agreement with this picture, which predicts an increasing  $u_{e+p}/u_B$  ratio with the hot spot distance.

## 5. Conclusions

A new XMM-Newton observation has solved the problem about the origin of the X-ray emission from the lobes of Pictor A. X-ray emission is due to IC scattering of CMB photons, confirming the study based on previous, suggestive but still uncertain, observations (Grandi et al. 2003, Hardcastle & Croston 2005, Kataoka & Stawarz 2005).

The IC magnetic field, estimated for each lobe, is a factor of 2.7 below equipartition value. A significant variation of key parameters, in the equipartition formula, can not account for this discrepancy: energetics of the lobes appear to be dominated by particles.

The good quality of the new observation has permitted a spatially resolved study of the lobes. Interesting results emerge from the study of the east lobe. In this case, an indication of an increase of magnetic field is registered in the region behind the east hotspot. A similar behaviour of the magnetic field is also considered in the model proposed by Hardcastle et al. (2005).

Moreover, when we combine the results of the two lobes, there is evidence for a correspondence between magnetic field and radio flux density variations. On the other hand, we do not observe a similar trend in electron density. Our results suggest a quite uniform distribution of particles in the lobes against a spatial variation of the magnetic field. This is in line with the figure of a magnetic field which decreases with the increasing distance from the hot spot proposed by Blundell & Rawlings (2000).

We are very grateful to R. Perley for kindly providing quantitatively analyzable radio images of Pictor A.

## REFERENCES

- Belsole,E., Worrall,D.M., Hardcastle,M.J., Birkinshaw,M., Lawrence,C.R., 2004, MNRAS 352, 924B
- Blumenthal,G.R., Gould, R.J., 1970, *RvMP*, 42, 237
- Blundell,K.M., & Rawlings,S., 2000, AJ, 119, 1111

- Blundell, K.M., Fabian A. C. Crawford C. S. et al. 2006 *ApJ* in press (astro-ph/0605391)
- Bondi, M., Brunetti, G., Comastri, A., Setti, G., 2004, *MNRAS*, 354L 43B
- Brunetti, G., Setti, G., Comastri, A., 1997, *A&A*, 325, 898
- Brunetti, G., Comastri, A., Setti, G., Feretti, L., 1999 *A&A* 342, 57B
- Brunetti, G., 2000 *APh* 13, 107B
- Brunetti, G., Cappi, M., Setti, G., Ferretti, L., Harris, D.E., 2001, *A&A*, 372, 755B
- Comastri, A., Brunetti, G., Dallacasa, D., Bondi, M., Pedani, M., Setti, G., 2003, *MNRAS*, 340L, 52
- Croston, J.H., Hardcastle, M.J., Harris, D.E., Belsole, E., Birkinshaw, M., 2005, *ApJ*, 626, 733
- Feigelson E.D., Laurent-Muehleisen S.A., Kollgaard R.I. and Fomalont E.B. 1995 *ApJ*, 449, L149
- Grandi, P., Guainazzi, M., Maraschi, L., Morganti, R., Fusco-Femiano, R., Fiocchi, M., Ballo, L., Tavecchio, F., 2003, *ApJ*, 586, 123
- Hardcastle, M. J., Birkinshaw, M., Cameron, R. A. et al., 2002, *ApJ*, 581, 948
- Hardcastle, M. J., Croston, J.H., 2005, *MNRAS*, 363, 649
- Harris D.E. & Grindlay J.E. 1979 *MNRAS* 188, 25
- Harris D.E., Krawczynski H, 2002, *ApJ*, 565, 244
- Isobe, N., Tashiro, M., Makishima, K., Iyomoto, N., Suzuki, M., Murakami, M.M., Mori, M., Abe, K., 2002, *ApJ*, 580, L111
- Isobe, N., Makishima, K., Tashiro, M., Hong, S., 2005, *ApJ*, 632, 781
- Kaneda, H., Tashiro, M., Ikebe, Y., Ishisaki, Y., Kubo, H., Makshima, K., Ohashi, T., Saito, Y., Tabara, H., Takahashi, T., 1995, *ApJ*, 453, L13
- Kataoka, J., Leahy, J.P., Edwards, P.G., Kino, M., Takahara, F., Serino, Y., Kawai, N., Martel, A.R., 2003b, *A&A* 410, 833
- Kataoka, J., Stawarz, L., 2005, *ApJ*, 622, 797
- Kraft, R.P., Forman, W.R. Jones, C., Kenter, A.T., Murray, S.S., et al., 2000, *ApJ*, 531L, 9

- Meisenheimer K., Yates M.G., Roeser H.-J., 1997, *A&A* 325, 57
- Mewe,R., Gronenschild, E.H.B.M., and van den Oord, G.H.J. 1985, *A&A*, 65, 511
- Miley, G., 1980, *ARA&A* 18, 165M
- Overzier,R.A., Harris,D.E., Carilli, Pentericci,L., et al, 2005,*A&A*, 433, 870
- Pacholczyk,A.,G., 1970, *Radio Astrophysics* (W.H. Freeman and Company: San Francisco)
- Perley R.A., Roser H.J. & Meisenheimer K. 1997 *A&A* 328, 12
- Ribickyi,G.B., Lightman,A.,P., 1979, *Radiative Processes in Astrophysics* (Wiley, New York)
- Reynolds,C.S., Sebastian,H., Begelman,M.C., 2001, *ApJ*, 549L, 179
- Robertson,J.G., 1973, *Aust.J.Phys* 26 403
- Tashiro M., Kaneda, H., Makishima, et al. 1998, *ApJ* 499, 713
- Tashiro M., Makishima, K., Iyomoto, N., Isobe, N., Kaneda, H., 2001, *ApJ*, 546, L19T
- Wilson, A.S., 2000, *AAS* 197.9401W
- Wilson A.S., Young A.J. & Shopbell P.L., 2001 *ApJ* 547, 740

## A. Checking the Equipartition Condition in the lobes

In this Appendix we use the equipartition formula revised by Brunetti et al. (1997) which accounts for a minimum energy of the emitting electrons,

$$B_{eq} = [C(\alpha)(1+k)\frac{L_{syn}(\nu)\nu^\alpha}{V}]^{\frac{1}{\alpha+3}}\gamma_{min}^{\frac{1-2\alpha}{\alpha+3}}, \quad (\text{A1})$$

where  $C(\alpha)$  is a quantity depending only from  $\alpha$ , we calculate equipartition magnetic fields,  $B_{eq}$ , for all the **W** and **E** lobes and compare them to the  $B_{IC}$  values estimated exploiting the IC scattering of the microwave background radiation by relativistic electrons. It is also necessary to stress that the adopted formula differentiates from the traditional one (Pacholczyk, 1970) where magnetic field is calculated in the frequency band between 10 and 100 MHz, corresponding to the frequency range observable with the radio telescopes.

At first, we assume  $\alpha = 0.8$ ,  $k = 1$  and  $\gamma_{min} = 50$  and a volume for each lobe region  $V = \text{Area (arcsec}^2) \times s$  where  $s$  is the path length, i.e the thickness of the analyzed region (see Table 2). The path length  $s$  is set equal to the lobe diameter ( $s = 95/h$  kpc) given by Perley et al. (1997), implicitly assuming a spherical geometry. Errors on  $B_{eq}$  are deduced by the propagation errors as done for  $B_{IC}$ , considering in this case the radio flux and Area uncertainties. Table 3 clearly shows that, even if the  $B_{eq}$  and  $B_{IC}$  trend are very similar, their values are not consistent. The magnetic fields based on equipartition condition overestimate  $B_{IC}$  by a factor  $\sim 3$ .

As it is well known, the influence of the unknown parameters can be important on the final result of  $B_{eq}$ , however our tests show that reasonable variations of a single parameter does not cause important changes in the  $B_{eq} / B_{IC}$  ratio. Indeed, the major uncertainty in the equipartition formula comes from our ignorance of  $\gamma_{min}$ . Clearly in the case of Pictor A  $\gamma_{min}$  cannot be much greater than several  $10^2$  as the synchrotron emission detected from the west radio hot spot at 74 MHz (Perley et al. 1997), and 330 MHz comes from  $\gamma \approx 800 - 10^3$  electrons (Meisenheimer et al. 1997) and adiabatic expansion from hot spots to the lobes should reduce the energy of these particles. According to Blundell’s calculations (Blundell et al. 2006), a reduction of a factor of 10 is expected for the Lorentz factors of all particles due to adiabatic expansion losses. Anyhow in the case of Pictor A it is  $B_{eq} / B_{IC} \propto \gamma_{min}^{-0.16}$  and even by adopting very conservative values  $\gamma_{min} \approx 800 - 10^3$  one would still find  $B_{eq} / B_{IC} \approx 1.9 - 1.7$ . Operating in the direction of a  $B_{eq}$  decreasing, we note that in the case of the east lobe  $k=0$  (assuming the contribution of heavy particles to be null) gives  $B_{eq} / B_{IC} \simeq 2.2$ , and  $s = 134$  kpc (accounting for projection effects for an inclination of the radio axis of  $\sim 45^\circ$ ) gives  $B_{eq} / B_{IC} \simeq 2.6$ . Analogous results are found for the west lobe. Even if all three parameters are simultaneously forced to the minimum value, we can not reach equipartition conditions.

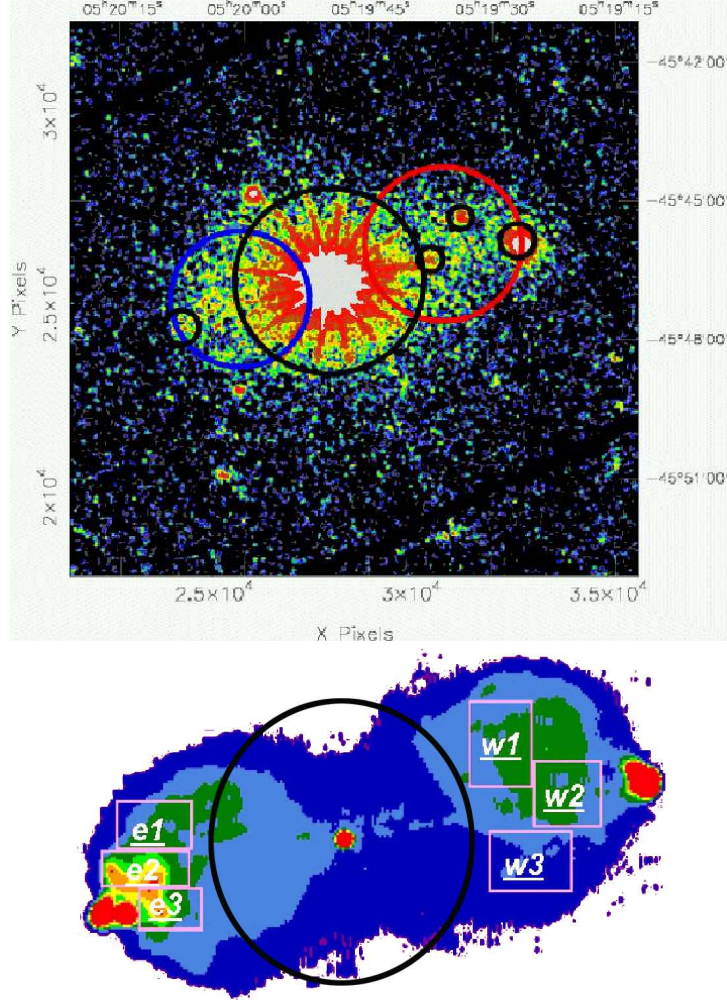


Fig. 1.— (*Upper Panel*) – *XMM-Newton* /MOS1 image (0.2-10 keV) of Pictor A observed on 14 January 2005. Several components are visible: the bright nucleus, the west hot spot, the jet and the two lobes. The blue and red circles represent the east (**E**) and west (**W**) extraction regions of the lobes, respectively. Regions (black circles) corresponding to the two hot spots, jet contribution and a point source, are excluded. (*Lower Panel*) – VLA map (Perley et al. 1997) at 20 cm. Pink boxes represent the sub-regions used for the spatially resolved analysis. Labels described in the text. Black circle delimitates the excluded nuclear region.

Table 1: XMM-Newton fit to the Western **W** and Eastern **E** Lobe of *Pictor A* in the 0.5-10 keV band.  $N_H$  is fixed to the galactic value  $N_H^{Gal} = 4.18 \times 10^{20} \text{ cm}^{-2}$

	Power Law			Thermal Emission		
	$\Gamma$	$\chi^2(\text{dof})$	Flux <sup>a</sup> (0.5-2 keV)	kT <sup>b</sup> (keV)	$\chi^2(\text{dof})$	Flux (0.5-2 keV)
<b>W</b>	$1.7^{+0.2}_{-0.2}$	29(38)	$12 \pm 1 \times 10^{-14}$	$6^{+3}_{-1}$	39(38)	$12 \pm 1 \times 10^{-14}$
<b>E</b>	$1.8^{+0.2}_{-0.2}$	33(31)	$9 \pm 1 \times 10^{-14}$	$5^{+3}_{-2}$	45(31)	$8 \pm 1 \times 10^{-14}$

<sup>a</sup> - X-ray Flux corrected for Galactic Absorption

<sup>b</sup> - Metal abundance fixed at 0.5

Table 2: Magnetic field and particles energy densities of the Western **W** and Eastern **E** Lobes and Spatially resolved Analysis Results:

	Flux <sub>1.4GHz</sub> (Jy)	Flux <sub>0.5-2keV</sub> (erg cm <sup>-2</sup> s <sup>-1</sup> )	Area (arcsec <sup>2</sup> )	$B_{IC}$ ( $\mu\text{G}$ )	$k_e$ ( $\times 10^{-5} \text{ cm}^{-3}$ )	$u_{e+p} / u_m$	$u_{e+p}$ ( $10^{-11} \text{ erg cm}^{-3}$ )
<b>East lobe</b>							
<b>E</b>	$11.4 \pm 0.3$	$9.0 \pm 1.0 \times 10^{-14}$	$12776 \pm 383$	$3.1 \pm 0.2$	$8.2 \pm 1.0$	$56 \pm 10$	$2.1 \pm 0.3$
<b>e1</b>	$2.5 \pm 0.1$	$1.9 \pm 0.3 \times 10^{-14}$	$2992 \pm 90$	$3.3 \pm 0.3$	$7.3 \pm 1.0$	$44 \pm 11$	$1.9 \pm 0.3$
<b>e2</b>	$2.8 \pm 0.1$	$1.2 \pm 0.2 \times 10^{-14}$	$1824 \pm 55$	$4.4 \pm 0.5$	$7.5 \pm 1.6$	$25 \pm 8$	$2.0 \pm 0.4$
<b>e3</b>	$2.5 \pm 0.1$	$1.5 \pm 0.2 \times 10^{-14}$	$1872 \pm 56$	$3.5 \pm 0.3$	$10.2 \pm 1.6$	$55 \pm 12$	$2.7 \pm 0.4$
<b>West lobe</b>							
<b>W</b>	$13.7 \pm 0.4$	$12.0 \pm 1.0 \times 10^{-14}$	$21408 \pm 642$	$2.9 \pm 0.2$	$6.5 \pm 0.8$	$50 \pm 10$	$1.7 \pm 0.2$
<b>w1</b>	$3.3 \pm 0.1$	$2.4 \pm 0.3 \times 10^{-14}$	$3640 \pm 109$	$3.2 \pm 0.3$	$8.0 \pm 1.4$	$51 \pm 13$	$2.1 \pm 0.4$
<b>w2</b>	$2.8 \pm 0.1$	$2.4 \pm 0.3 \times 10^{-14}$	$3024 \pm 91$	$3.2 \pm 0.3$	$8.1 \pm 1.4$	$52 \pm 13$	$2.1 \pm 0.4$
<b>w3</b>	$1.5 \pm 0.1$	$2.9 \pm 0.5 \times 10^{-14}$	$3400 \pm 102$	$2.5 \pm 0.2$	$7.7 \pm 1.1$	$81 \pm 17$	$2.0 \pm 0.3$

<sup>a</sup> – Radio flux uncertainties of 3% reflect calibration uncertainties of the antenna

<sup>b</sup> –Areas of each sub-region are measured using the 20 cm radio map. See also Fig. 1 (*Lower Panel*)

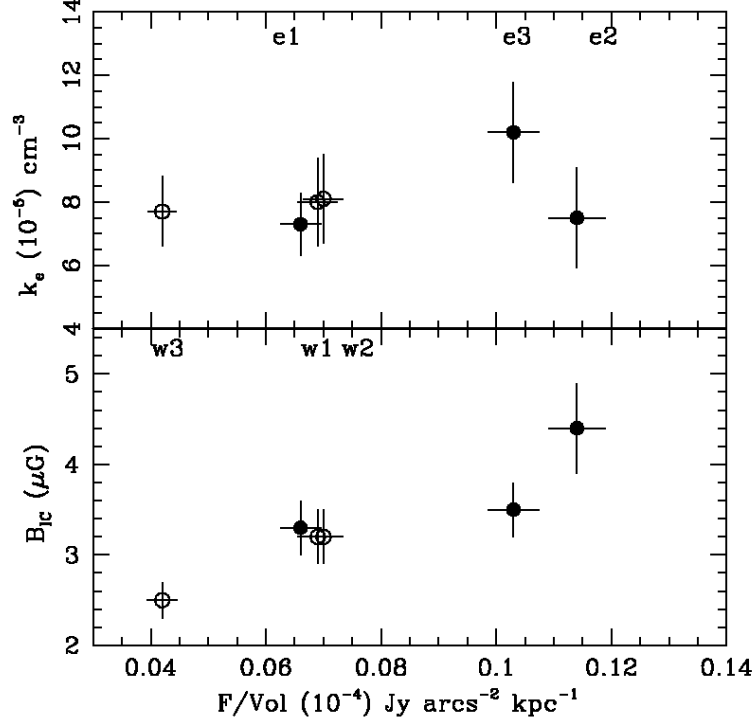


Fig. 2.—  $B_{IC}$  (*Lower Panel*) and  $k_e$  (*Upper Panel*) values of east (solid circles) and west (empty circles) sub-regions are plotted as a function of the radio flux ( $F/V$ ) at 1.4 GHz, normalized by the relative volume.

Table 3: Equipartition magnetic fields ( $B_{eq}$ ), calculated with the revised determined formula by Brunetti et al.(1997), and their ratios with the relative  $B_{IC}$ .

	E	W
$B_{eq}$ ( $\mu$ G)	$8.7 \pm 0.1$	$8.8 \pm 0.1$
$B_{eq} / B_{IC}$	$2.8 \pm 0.2$	$2.7 \pm 0.2$